Journal of the Serbian Chemical Society
JSCS-info@shd.org.rs • www.shd.org.rs/JSCS

ACCEPTED MANUSCRIPT

Journal of the Serbian Chemical Society
JSCS-info@shd.org.rs • www.shd.org.rs/JSCS
J. Serb. Chem. Soc. **00(0)** 1-24 (2026)
JSCS–13631
Original scientific paper
Published DD MM, 2026

Phenolic compounds adsorption from olive oil industry effluent using experimental design methodology: screening and central composite design optimization

NOUARA YAHIAOUI[1]*, RACHIDA DOUANI[1], M'HAND OUGHANEM[1], NOUARA LAMRANI[1†], KAHINA IKKOUR[1,2], SADIA DEKKAR[1]

[1]*Laboratory of Applied Chemistry and Chemical Engineering, Faculty of Exact Sciences, University Mouloud MAMMERI of Tizi-Ouzou, 15000 Tizi-Ouzou, Algeria,* [2]*Laboratory of Physico-Chemical of Materials and Catalysis, Faculty of Exact Sciences, University of Béjaïa, Algeria.*

(Received 15 November 2025; revised 17 January 2026; accepted 31 July 2026)

Abstract: The experimental design methodology was investigated to model and optimize the adsorption process for removing phenolic compounds (PC) from olive mill wastewater (OMW) using magnesium-aluminum layered double hydroxide (LDH). The LDH powders were synthesized by the co-precipitation method. The structural, textural and morphological characterizations were performed. To evaluate quickly and effectively the effects of five parameters (initial PC content, contact time, solid/liquid (S/L) ratio, initial pH, and temperature) on the adsorption efficiency, a Hadamard matrix was employed for screening. Subsequently, a central composite design (CCD) was utilized to optimize the adsorption process based on four key parameters. The correlation coefficient for the polynomial model was found to be 94%. Predicted values generated from the response function matched the experimental data closely, indicating a good agreement. Under the selected optimal conditions, a maximum PC removal efficiency of 80.85 % was achieved. The reusability of the regenerated LDH by calcination at 500 °C in the adsorption process was assessed over four consecutive runs under the selected optimal conditions. The removal percentages of PC and chemical oxygen demand (COD) indicated that calcined LDH could be a viable alternative for treating OMW.

Keywords: olive mill wastewater; magnesium-aluminum layered double hydroxide; chemical oxygen demand; Hadamard matrix; regeneration.

INTRODUCTION

The olive oil industry is constantly innovating to improve the oil production process in Mediterranean countries. Paradoxically, this industry generates by-

* Corresponding authorc. E-mailc: nouara.yahiaoui@ummto.dz; †nouara.lamrani@ummto.dz.
https://doi.org/10.2298/JSC251115043Y

products with a high environmental impact, in particular olive mill wastewater (OMW).[1] OMW constitutes the residual liquid effluent from the two- or three-phase extraction process, which is characterized by a high pollution load due to its high content of biodegradable organic matter, toxic phenolic compounds, suspended solids and fatty compounds.[2] Every year, olive-growing countries produce large quantities of this effluent. In Algeria, the production of 30,000 tons of olive oil generates 105,000 tons of OMW.[3]

The polluting activity of OMW is linked with its high organic load represented especially by an important phenol compound content, a very high chemical oxygen demand (COD), an equally high biological oxygen demand BOD_5 and an acid pH.[4]

As a source of harmful pollution to the environment, OMW must be treated to remove the phenolic content fraction before being discharged in receiving water bodies or soils. Among the various studied approaches proposed for treating this effluent, chemical processes offer effective solutions for reducing its toxicity. Techniques such as advanced oxidation (Fenton, electro-oxidation, ozonation, etc.),[5-6] coagulation-flocculation,[7] adsorption on activated materials[8] and co-precipitation[9]were used to degrade or extract the PC responsible of OMW's pollutant load.

The adsorption technique is a promising technology widely used for treating various types and removing pollution from the environment. Its advantages include simplicity, short treatment, ease of operation and handling, high efficiency and the ability to regenerate adsorbents.[10-11]

Activated carbon was considered as a primary adsorbent for removing organic and inorganic pollutants from wastewater due to its high specific surface area. However, the high costs of manufacturing and regenerating after saturation limit its widespread use. To find alternatives, several studies have explored inorganic adsorbents that are more accessible and cost-effective, offering increased regenerability and recyclability, which is crucial for sustainable large-scale applications for treating wastewater, including OMW. In this sense, Yahiaoui *et al.*[9] studied the co-precipitation of PC and organic matter from OMW using synthetic hydroxyapatite as adsorbent, achieving reduction rates of 87.30% for PC and 76.30% for COD. Additionally, Beccari *et al.*[12] demonstrated that bentonites can reduce the chemical oxygen demand (COD) of OMW by approximately 61.6% at a pH of 6.5. Other researchers applied this adsorption process to Fes clays and, after optimizing the treatment system, achieved a COD reduction rate of nearly 86%.[13]

Lamellar double hydroxides, whether in their original form or after thermal decomposition, represent a unique family of clay materials characterized by distinct chemical and physicochemical properties, such as varied composition, easy synthesis, low cost, low toxicity, and high specific surface area. The general formula of the LDH materials is $[M_{1-x}M'_x\ (OH)_2]^{x+}(X)_{x/m}nH_2O$, where M and M'

are bivalent and trivalent cations, respectively, with similar radii, and X is the interlayer anion. The cations in the layer can be changed using a wide range of main group cations (Mg and Al) or transition metal cations (V, Zn, Cr, Mn, Fe, Co, Ni…). All these materials, having various compositions, share typical common characteristics: layered structure and the formation of mixed-metal oxides after thermal treatment.[14] Moreover, the "memory effect" is a very interesting property of this kind of compound that is based on the ability of the oxides derived from the calcination of LDH in reconstructing, the layer structure when rehydrated in the presence of anions.[15] Consequently, the literature has documented numerous studies related to their applications in industrial, medical, and environmental fields.[16-17]

Due to their high specific surface area and the flexibility of their inter-filament space, LDHs can effectively trap negatively charged species through surface adsorption and anion exchange, such as nitrate, phosphate, and chromate anions,[18] as well as toxic molecules like agricultural pesticides[19] from wastewater. Several researchers have utilized these compounds as adsorbents for PC in OMW.[20-21] The obtained results showed that the adsorption capacity is significantly influenced by the nature and structure of the LDHs used. A study conducted by Zhang *et al.*[22] demonstrated that aluminum- and magnesium-based LDHs (Mg-Al LDHs) have a strong affinity for anionic compounds due to their exceptional stability and high positive charge density. Their structure is similar to that of the natural LDH known as brucite, making them environmentally friendly, non-toxic, and cost-effective.[23] Calcining these LDHs at temperatures between 400 and 600 °C produces mixed oxides with high porosity and specific surface area. Additionally, the memory effect resulting from hydration enhances their adsorption capacity for both organic and inorganic compounds.[15]

These interesting results led us to investigate and optimize the adsorption efficiency of magnesium-aluminum LDH, and its calcined product at 500°C (LDH-500), in reducing the load of PC from OMW using experimental design methodology.

The experimental design approach is a powerful tool for understanding and optimizing experimental parameters by combining multiple variables in a single study; rather than conducting separate studies for each one, the number of required trials is significantly decreased. This approach allows for the extraction of more information with less experimentation, ultimately leading to reduced costs.[24]

The centred composite design (CCD) is one of the methods used in response surface methodology (RSM) that allows for the study of a phenomenon across a broad experimental range. This is achieved by including axial points, which enhances the reliability and accuracy of the modeling, especially when interaction and quadratic effects are present, all while minimizing the number of required experiments.[24]

This study aims to optimize the adsorption process for the removal of PC from OMW by using experimental design. Consequently, an empirical relationship (a second-degree polynomial) was established using CCD to calculate the optimal rate of PC removal accurately. The reusability of the LDH was also investigated.

EXPERIMENTAL

Fresh OMW used in this study was obtained by crushing Chemlal olives harvested during the 2024/2025 olive growing season. This vegetation water was extracted using a continuous system at a modern oil mill located in Tizi-Ouzou, northern Algeria.

To remove solids and fats, the raw OMW was first filtered and then centrifuged at 5000 rpm for 20 minutes, to eliminate suspended matter. The mixture was further decanted using a separating funnel to remove any remaining fat. The pretreated and homogenized OMW was stored in plastic bottles in a freezer at -5°C until needed. Table I presents the main characteristics of the effluent.

The measured chemical oxygen demand (COD) of the crude OMW was 167 $gO_2 \cdot L^{-1}$, indicating a high concentration of organic matter, particularly PC (4.21 $g \cdot L^{-1}$). This value is significantly higher than those reported in the literature by Yahiaouiet *et al.*[9] and Lateb *et al.*[7], which recorded COD values of 86 $gO_2 \cdot L^{-1}$ and 131 $gO_2 \cdot L^{-1}$, respectively. The discrepancy can be attributed to differences in the nature and/or method of olive crushing used during oil extraction.

TABLE I. Physico-chemical characteristics of OMW

Parameter	Unit	value
pH	-	4.96
Conductivity	$mS \cdot cm^{-1}$ at 25°C	16.42
Turbidity	NTU	109
Dry matter content	$g \cdot L^{-1}$	49.25
Water content	%	95.02
Ashes	$g \cdot L^{-1}$	5.75
Volatile matter content	$g \cdot L^{-1}$	43.50
Chemical oxygen demand (COD)	$gO_2 \cdot L^{-1}$	167
PC content	$g \cdot L^{-1}$	4.21

LDH with chloride in the interlayer particles was prepared by a direct co-precipitation process at room temperature following the procedure described previously by Ulibarri *et al.*[25] Briefly, A solution containing $MgCl_2$ (0.25 $mol \cdot L^{-1}$) and $AlCl_3$ (0.125 $mol \cdot L^{-1}$) was added dropwise under vigorous stirring at room temperature to NaOH solution at pH 10. The suspension was kept at this pH by adding 2 $mol \cdot L^{-1}$ Na_2CO_3 solution. After complete addition, the resulting mixture was aged for 24 h under thermal treatment at 80°C. The obtained precipitate was washed several times with distilled water, then recovered by vacuum filtration through a porcelain funnel containing a filter cloth. The obtained compound was dried in an oven at 70°C for 24 hours. The prepared LDH was crushed, and sieved to have a uniform particle size, and calcined at 500°C in an oven for 4 hours, to improve the structural properties and those of porous exchange. The final compound is denoted LDH-500.

Characterization

The surface morphology of the synthesized LDH and LDH-500 was performed using a scanning electron microscope (SEM) (PHILIPS ESEMXL30 with tungsten filament). The elemental composition of the powder's surface was analyzed by energy dispersive spectroscopy (EDS).The specific surface area, volume, and mean pore diameter of the powder particles were measured through a nitrogen physisorption at −196 °C using a Quantachrome Nova 2000e apparatus. The specific surface area was determined using the Brunauer–Emmet–Teller (BET) method; while the average pore volume was calculated using the Barrett–Joyner–Halenda (BJH) method.

The crystalline structure was analyzed via X-ray diffraction (Panalytical Empyrean X-ray diffractometer with Cu Kα(1.5406 Å) radiation at 45 kV) over a 2θ range of 0° to 80°.The synthesized particles were also characterized by Raman spectroscopy (spectrometer from Renishaw) using a visible laser with a wavelength of 632.8 nm.

The infrared spectroscopic analysis was conducted using a SHIMADZU brand FTIR8400 Fourier transform spectrophotometer in the wavenumber range of 400- 4000 cm^{-1} to identify the functional groups present in the products.

Sorption experiments

Preliminary tests were performed to identify the most effective adsorbent. Specifically, we investigated the batch adsorption of PC from OMW using LDH and LDH-500 over different time intervals. A mass of 0.5 g of each adsorbent was added to 25 mL of OMW, and the mixture was continuously stirred at 300 rpm for contact times ranging from 5 to 120 minutes.

Sorption experiments for PC were conducted in 200 mL glass beakers using two doses (1 g and 10 g) of LDH-500 mixed with 100 mL of OMW at varying concentrations of PC (1.40 $g{\cdot}L^{-1}$ and 2.80 $g{\cdot}L^{-1}$). The pH of the solutions was adjusted to 7 and 12 by adding a 2 M NaOH solution. The mixture was continuously stirred at 300 rpm for 5 and 90 minutes at temperatures of 25°C and 45°C. Once the designated contact time was reached, the suspension was centrifuged at 5000 rpm for 10 min. The recovered supernatant was analyzed for PC content, $g{\cdot}L^{-1}$ by the Folin–Ciocalteu colorimetric method using gallic acid for calibration, as described by Macheix*et al.*[26] The analysis were expressed as gallic acid equivalents, with $R^2 = 0.996$.

The percentage removal R, % of PC was calculated using the following equation:

$$R = \frac{C_0 - C_f}{C_0} \times 100 \quad (1)$$

C_0 and C_f, $g{\cdot}L^{-1}$ represent the initial and final concentrations of the PC, respectively.

A study was conducted using experimental design methodology (EDM) to quickly and accurately identify the factors that significantly affect the PC removal rate. The process began with screening the factors, followed by optimization. This step aims to identify the factors that significantly influence the removal rate of PC from OMW. To estimate the weight of each factor, a Hadamard matrix was implemented.[27] Table II presents the factors considered and their corresponding experimental domains.

In screening factors with a Hadamard matrix, the number of experiments, N, must be a multiple of 4 and should satisfy the condition $N \geq k + 1$. In our study, with $k = 5$, the minimum number of experiments required was $N = 8$. However, this experimental design didn't provide enough degrees of freedom to accurately calculate the experimental variance and assess with precision the significance of the factors' effects. To resolve this issue, we doubled the design to $N = 16$ experiments.[24,28] Table III presents the experimental matrix using both coded and real variables. The response being investigated is the PC removal percentage, denoted as R.

TABLE II. Factors and their levels in experimental design

Factor	Unit	Symbol	Code	Level (-)	Level (+)
Contact time	min	τ	X_1	5	90
Solid/liquid ratio (S/L ratio)	$g{\cdot}L^{-1}$	S/L	X_2	1	10
pH	-	pH	X_3	7	12
Temperature	°C	T	X_4	25	45
Initial PC content	$g{\cdot}L^{-1}$	C	X_5	1.40	2.80

TABLE III. Design matrix of screening and results obtained for the studied response (R)

Run	Code variables					Real variables					R/ %
	X_1	X_2	X_3	X_4	X_5	τ	S/L	pH	T	C	
1	1	1	1	-1	1	90	10	12	25	2.80	83.45
2	1	1	1	-1	1	90	10	12	25	2.80	79.14
3	-1	1	1	1	-1	5	10	12	45	1.40	33.81
4	-1	1	1	1	-1	5	10	12	45	1.40	25.18
5	-1	-1	1	1	1	5	1	12	45	2.80	76.26
6	-1	-1	1	1	1	5	1	12	45	2.80	74.10
7	1	-1	-1	1	1	90	1	7	45	2.80	56.47
8	1	-1	-1	1	1	90	1	7	45	2.80	54.68
9	-1	1	-1	-1	1	5	10	7	25	2.80	67.27
10	-1	1	-1	-1	1	5	10	7	25	2.80	73.02
11	1	-1	1	-1	-1	90	1	12	25	1.40	49.64
12	1	-1	1	-1	-1	90	1	12	25	1.40	43.17
13	1	1	-1	1	-1	90	10	7	45	1.40	10.43
14	1	1	-1	1	-1	90	10	7	45	1.40	15.11
15	-1	-1	-1	-1	-1	5	1	7	25	1.40	33.09
16	-1	-1	-1	-1	-1	5	1	7	25	1.40	39.92

The four parameters used for this modeling were selected based on the results of the screening experiments for the central composite design: S/L ratio, pH, temperature, and initial PC content, referred to coded variablesX_2, X_3, X_4, and X_5, respectively. A centered composite matrix with four factors was employed to develop the mathematical model, enabling the calculation of response values throughout the experimental domain.[24] The experimental range of factors was consistent with that established in the screening stage (Table II). This matrix comprises N=34 experiments, which are divided into:

$N_f = 2^4 = 16$ factorial points;

$N_\alpha = 2*4=8$ axial points;

$N_0 = 5$ central points (to determine the experimental variance);

$N_t = 5$ test points (to check the validity of the postulated model);

The postulated mathematical model, which is a polynomial of the second degree, is given by the following equation:

$$\grave{R} = a_0 + a_2X_2 + a_3X_3 + a_4X_4 + a_5X_5 + a_{22}X_2^2 + a_{33}X_3^2 + a_{44}X_4^2 + a_{55}X_5^2 + a_{23}X_2X_3 + a_{24}X_2X_4 + a_{25}X_2X_5 + a_{34}X_3X_4 + a_{35}X_3X_5 + a_{45}X_4X_5 \quad (2)$$

where X_2, X_3, X_4 and X_5 represent the coded variables of the system; a_0, a_i ($i=2,3,4,5$), a_{ii} ($i=2,3,4,5$) and a_{ij} ($i=2,3,4$; $j=3,4,5$) are the regression coefficients for intercept, linear, quadratic and interaction terms, respectively. Table IV displays the experimental matrix,

including both coded and real values as well as the response values for all experiments. The experimental data were used to estimate the model coefficients via the least squares method with Nemrodw software (version 2007.3).[29]

TABLE IV. Central composite design and the resulting experimental results obtained for the response (R)

Run	Coded variables				Real variables				R / %
	X_2	X_3	X_4	X_5	S/L	pH	T	C	
1	-1	-1	-1	-1	1.00	7.00	25.00	1.40	77.70
2	+1	-1	-1	-1	10.00	7.00	25.00	1.40	78.42
3	-1	+1	-1	-1	1.00	12.00	25.00	1.40	79.86
4	+1	+1	-1	-1	10.00	12.00	25.00	1.40	79.14
5	-1	-1	+1	-1	1.00	7.00	45.00	1.40	78.10
6	+1	-1	+1	-1	10.00	7.00	45.00	1.40	76.26
7	-1	+1	+1	-1	1.00	12.00	45.00	1.40	78.42
8	+1	+1	+1	-1	10.00	12.00	45.00	1.40	79.86
9	-1	-1	-1	+1	1.00	7.00	25.00	2.80	44.60
10	+1	-1	-1	+1	10.00	7.00	25.00	2.80	43.88
11	-1	+1	-1	+1	1.00	12.00	25.00	2.80	42.25
12	+1	+1	-1	+1	10.00	12.00	25.00	2.80	49.76
13	-1	-1	+1	+1	1.00	7.00	45.00	2.80	37.41
14	+1	-1	+1	+1	10.00	7.00	45.00	2.80	41.01
15	-1	+1	+1	+1	1.00	12.00	45.00	2.80	41.01
16	+1	+1	+1	+1	10.00	12.00	45.00	2.80	42.45
17	-1	0	0	0	1.00	9.50	35.00	2.10	59.71
18	+1	0	0	0	10.00	9.50	35.00	2.10	56.83
19	0	-1	0	0	5.50	7.00	35.00	2.10	70.75
20	0	+1	0	0	5.50	12.00	35.00	2.10	64.62
21	0	0	-1	0	5.50	9.50	25.00	2.10	64.62
22	0	0	+1	0	5.50	9.50	45.00	2.10	57.11
23	0	0	0	-1	5.50	9.50	35.00	1.40	66.46
24	0	0	0	+1	5.50	9.50	35.00	2.80	47.77
25	0	0	0	0	5.50	9.50	35.00	2.10	59.00
26	0	0	0	0	5.50	9.50	35.00	2.10	59.00
27	0	0	0	0	5.50	9.50	35.00	2.10	59.71
28	0	0	0	0	5.50	9.50	35.00	2.10	52.52
29	0	0	0	0	5.50	9.50	35.00	2.10	57.57
30	-0.40	-0.23	-0.16	-0.13	3.72	8.93	33.39	2.01	58.64
31	+0.40	-0.23	-0.16	-0.13	7.28	8.93	33.39	2.01	59.26
32	0	+0.46	-0.16	-0.13	5.50	10.64	33.39	2.01	61.15
33	0	0	+0.48	-0.13	5.50	9.50	39.84	2.01	51.14
34	0	0	0	0.50	5.50	9.50	35.00	2.45	49.61

RESULTS AND DISCUSSION

Fig.1 displays SEM micrographs and EDS spectra of LDH powders synthesized before (Fig.1 a-c) and after (Fig.1 d-f) calcinations at 500°C. The samples exhibit irregular morphology, with grains stacked in layers, indicating the formation of a lamellar structure. As shown in Fig.1 d, the flat stacked structure was maintained after the calcination process. However, a reduction in particle size was observed and the resulting particles formed agglomerates. The EDS spectra reveal the presence of O, Al, Mg, Cl, and C. Compared to LDH, the LDH-500 sample shows a slight decrease in Cl, Na and C content probably due to the rinsing process for Cl and Na and desorption of carbon dioxide from the surface of the formed oxides for C content. The results of the elemental composition of the powder surface analysis were summarized in Table V.

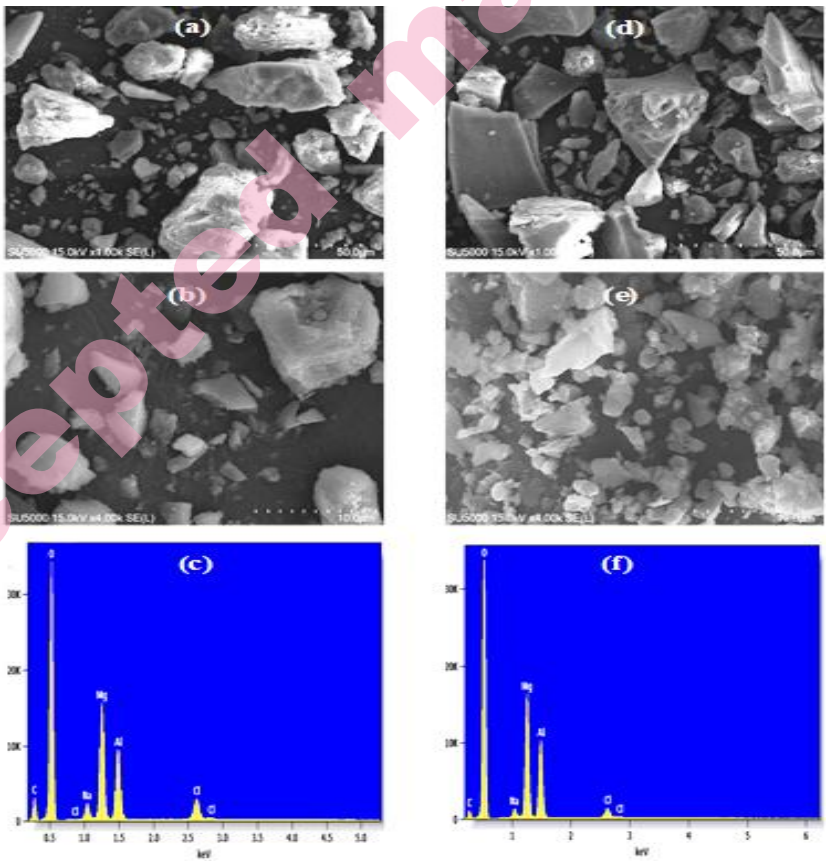

Fig 1. SEM images and EDS spectra of (a–c) LDH and (d–f) LDH-500 samples.

TABLE V. Quantitative results of LDH and LDH-500 powders

Element	Weight / %	
	LDH	LDH-500

		Average porous volume / $cm^3 \cdot g^{-1}$	Average pore diameter / nm
LDH	45,67	0,085	3,73
LDH-500	46,38	0,107	4,65

X-ray diffraction (XRD) analysis was performed on both the layered double hydroxide (LDH) and the LDH-500. Fig. 2 displays the corresponding diffraction patterns. Phase identification and diffraction peak indexing, conducted using High'Score-Plus software, reveal a predominant phase corresponding to dialuminum tetramagnesium dodecahydroxide trihydrate, with the chemical formula $Mg_4Al_2(OH)_{12}CO_3$ $3H_2O$, as referenced in the JCPDF database under [98−017−2994]. This phase crystallizes in a hexagonal lattice (R3m symmetry), characteristic of double-layer hydroxides.

The characteristic peaks of LDHs are observed at low angles of $2\theta = 11.81°$ and 23.53°, corresponding to the (003) and (006) planes, respectively. These peaks indicate the interlayer spacing of the material and illustrate the lamellar structure of LDHs. A high value of $d_{003} = 7.587$ Å, typical for hydrated carbonate LDH, confirms the presence of water molecules and carbonate anions (CO_3^{2-}) in the interlayer space of the structure.[30]

Additionally, indexing reveals peaks corresponding to aluminum oxide (II) (AlO) with a cubic structure (JCPDF [01−075−0278]), where the main peak (200)

is observed at 2θ = 31.86°, corresponding to an interlayer spacing of approximately 2.83 Å. This phase may result from partial decomposition or impurities in the LDH material during synthesis.

The presence of the hydrated LDH phase in both samples enhances the adsorption of PC, as the layered structure and hydroxylated surface provide numerous sites for ion exchange and hydrogen bonding interactions.[31]

The XRD pattern of LDH-500 shows additional peaks attributed to the formation of a spinel phase Al_2MgO_4 (JCPDF [98-009-6839]) and magnesium oxide (MgO, JCPDF [98-016-2607]). These phases appear after calcination at 500°C, which induces the decomposition of the hydrated LDH phase and the recombination of the oxides.

It is important to note that the intensity of the characteristic peaks of the hydrated phases (LDH and AlO) decreases, indicating a partial loss of crystallinity and the thermochemical transformation of the material during heat treatment.

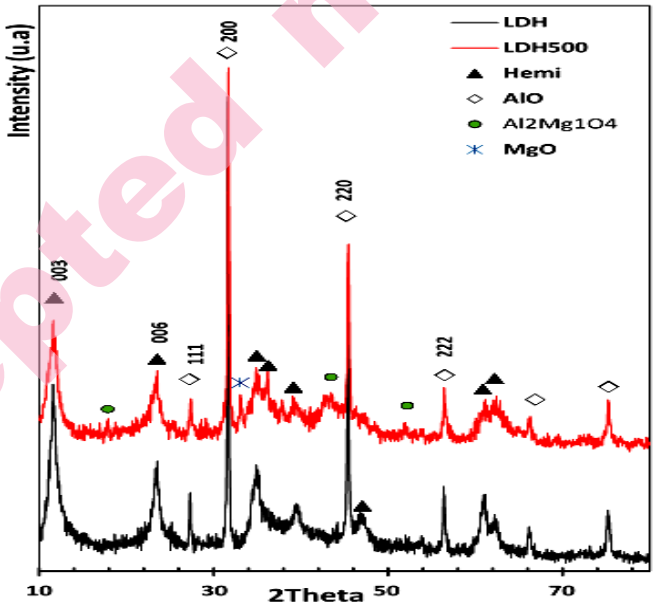

Fig 2. X-raydiffraction patterns of LDH and LDH-500 samples

The Raman spectra obtained for the samples are illustrated in Fig. 3. They reveal several characteristic bands corresponding to the phase identified by XRD as $Mg_4Al_2(OH)_{12}CO_3\ 3H_2O$. The intense band observed around 1060 cm^{-1} for LDH and the band at approximately 1057 cm^{-1} for LDH-500 correspond to the symmetric ν_1 stretching mode of the carbonate group CO_3^{2-} intercalated between the layers. This is in good agreement with the values reported for similar carbonate hydrotalcites. Frost *et al.*[32] report peaks between 1055 and 1086 cm^{-1} for

carbonated LDHs, while Frederick *et al.*[33] identify two distinct bands at 1046 and 1062 cm^{-1} for natural quintinite. A clear band at 560 cm^{-1} can be attributed to M–O or M–OH vibrations in the octahedral layers, involving Mg–O and Al–O bonds.[34-35] These studies systematically associate this spectral range (540–560 cm^{-1}) with the vibrational modes of the hydroxyl network. Finally, the presence of a low-frequency mode around 150-155 cm^{-1}, which is rarely discussed in the literature, can be interpreted as an M-O-M deformation vibration[34-36]or as OH vibrations.[32]

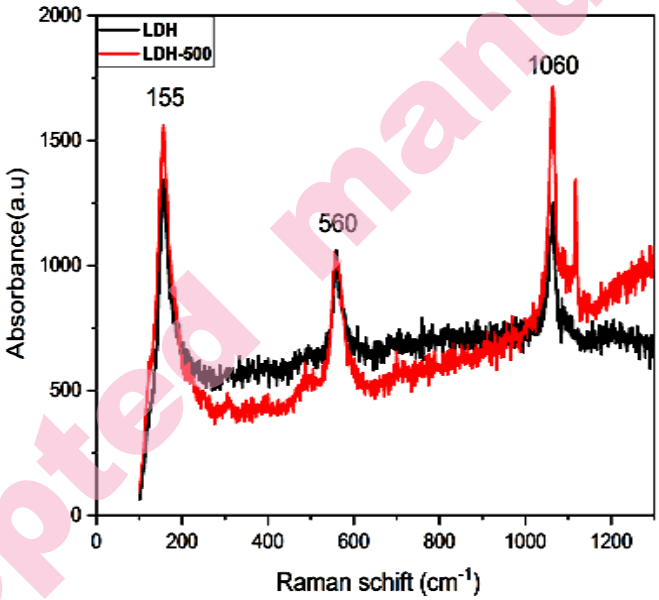

Fig 3. Raman spectra of LDH and LDH-500 samples

As shown in Fig. 4, the infrared spectra of the hydrotalcite samples exhibit characteristic bands of the double-lamellar hydroxide phase. In the uncalcined sample, the intense band at 3375 cm^{-1}, is attributed to O-H stretching vibrations of hydroxyl groups, water molecules within the lamellar structure, and physically adsorbed water.[37] The significant band around 1348 cm^{-1} is associated with the presence of carbonate anions CO_3^{2-} in the interlayer galleries.[38] The bands observed around 947, 783, and 551 cm^{-1}correspond to metal-oxygen stretching modes.[21]Additionally, Luiz. *et al.*[39]attributed the band near 653 cm^{-1} to Mg-O or Al-O bonds. After calcination, a decrease in the intensity of most previously mentioned bands was observed. The reduction in intensity in the spectral region, corresponding to hydroxyl (OH) groups indicates dihydroxylation and the conversion of metal hydroxides to metal oxides.[21] Additionally, the decrease in intensity of the band at 1348 cm^{-1}, associated with interlayer carbonates, can be

attributed to the desorption of carbon dioxide from the surface of the formed oxides.[40] This result is consistent with that of EDS, XRD and Raman results.

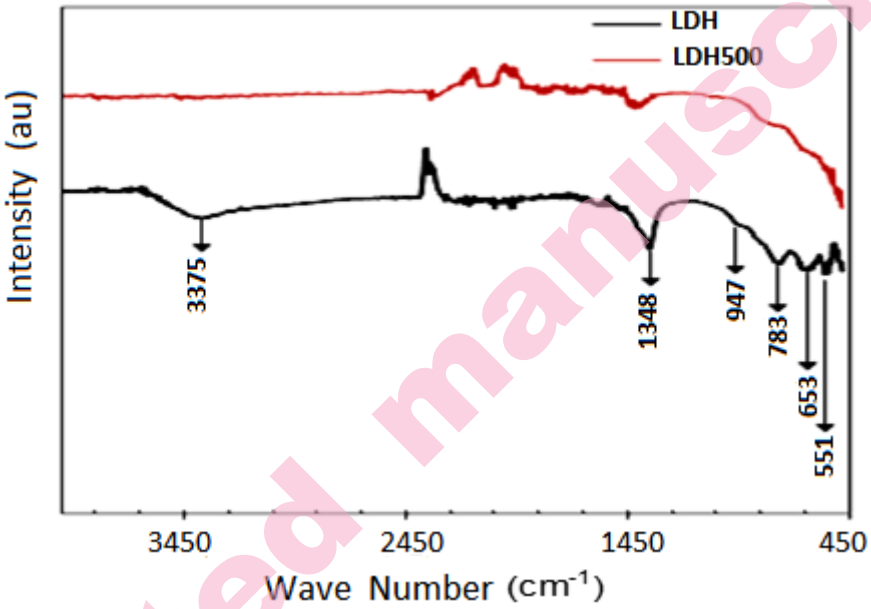

Fig 4. FTIR spectra of LDH and LDH-500 samples

The kinetic adsorption results shown in Fig. 5 reveal that calcined LDH-500 achieved the highest elimination rate of 70.40 % for PC within just 5 minutes. In contrast, LDH reached equilibrium after 60 min, with an elimination rate of 63.50%. The higher adsorption capacity of LDH-500 can be attributed to its larger porous surface area developed during thermal treatment, which promoted the formation of metal oxides.[41] Additionally, the memory effect, which upon rehydration gave a native LDH with increased adsorption capacity.[42]

Referring to the literature data, particularly the research on LDHs, the rapid adsorption followed by a plateau observed in the case of LDH-500 indicates a two-step mechanism. This mechanism involves initial surface adsorption followed by a second step controlled by diffusion, which typically aligns with second-order or interaparticle diffusion kinetic models.[21, 43-44]

Based on these findings, calcined LDH-500 was chosen for the subsequent phase focused on optimizing the adsorption process for PC using experimental designs.

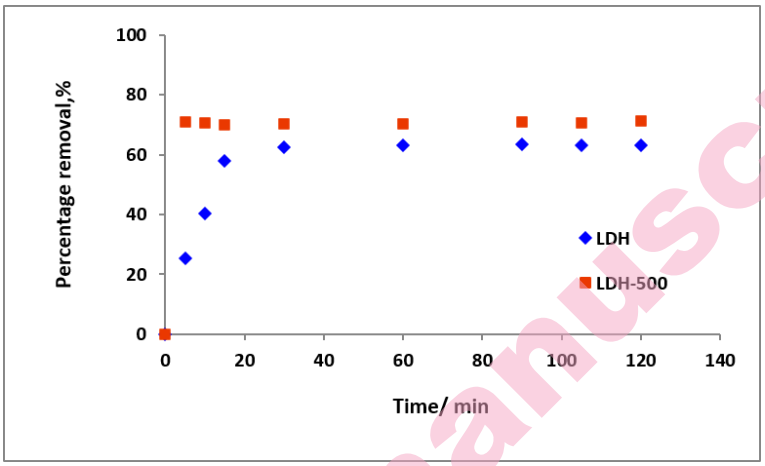

Fig 5. Removal percentage of PC over time

The experimental values of the response R (Table 3) were used in screening to determine the coefficients b_1, b_2, b_3, b_4 and b_5, which represent the weights associated to the variables t, S/L, pH, T, and C, respectively; b_0 is the intercept.

Using the Student's t experimental (t_{exp}) and the degrees of freedom (ddl), the significance level (%) was determined according to Student's t-distribution. The coefficients and other statistical parameters were calculated with Nemrodw software.[27] The results are presented in Table VII.

TABLE VII. Estimates and statistics of coefficients (screening)

Name	Coefficient	Inflation factor	Standard deviation	t.exp	Signif / %
b_0	50.921	-	0.891	57.13	< 0.01 [b]
b_1	-1.910	1.00	0.891	-2.14	5.8
b_2	-2.495	1.00	0.891	-2.80	1.88 [a]
b_3	7.173	1.00	0.891	8.05	< 0.01[b]
b_4	-7.666	1.00	0.891	-8.60	< 0.01 [b]
b_5	19.627	1.00	0.891	22.02	< 0.01[b]

[a] Significant at the level of 95%; [b] Significant at the level of 99.9%

It is established that an effect is considered significant if the significance level is below 5%. The results presented in Table 7 indicate that initial PC content, pH, S/L ratio, and temperature were the main factors influencing the response. However, the contact time had no significant effect (p=5.8%) on the PC removal. Fig 6 presents the Pareto chart established to support these statistical results and showed the standardized effects in decreasing order as follows: initial PC content (76.24) > temperature (11.63) > pH (10.18) > S/L ratio (1.23) > contact time (0.72), clearly indicating that contact time didn't influence the retention of PC by

this material. Therefore, the contact time for the remainder of the study was fixed at its minimum level of 5 min.

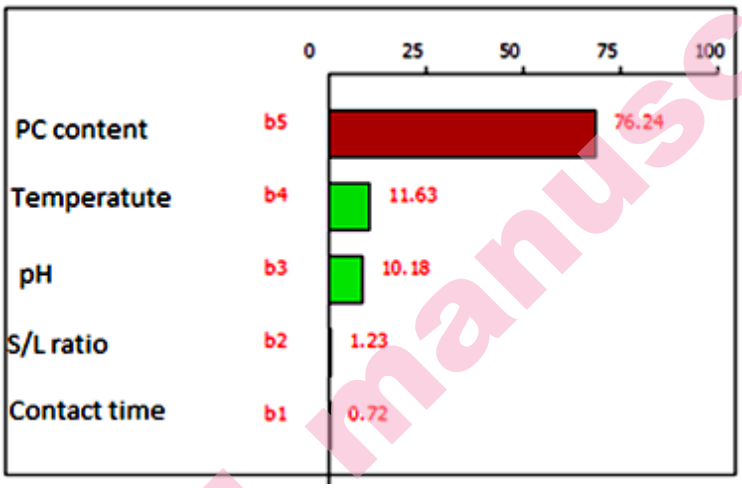

Fig 6. Pareto chart displaying the standardized effects of factors (screening)

Before carrying out experiments, it is necessary to verify the quality of prediction given by the variance function and isovariance by rotation.

A variance function (d) is considered to provide an acceptable prediction if its maximum value, d_{max}, is less than or equal to unity $d_{max} \leq 1$, in the studied matrix, $d_{max} = 0.79$. Since this value is less than unity, any response predicted by the model within the experimental domain will have an accuracy that is at least equal to that obtained from actual experiments. Additionally, the isovariance by rotation was verified, indicating that the responses calculated by the postulated model had the same prediction error for all the points located at the same distance from the center of the studied domain (Fig. 7).

To establish the mathematical model that describes the relationship between the factors, a central composite design was applied in the experimental domain outlined in Table 2. The experimental results for the response R, as shown in Table IV, were used to determine the 15 coefficients of the second-degree polynomial model, without the inclusion of checkpoints.

The coefficient of determination of 0.95 and the adjusted determination coefficient of 0.91 indicate that the model fits well. The postulated model, expressed in coded variables, is represented by the following equation:

$$R = 59.21 + 0.51\, X_3 - 16.89\, X_5 + 7.10\, X_3^2 \quad (3)$$

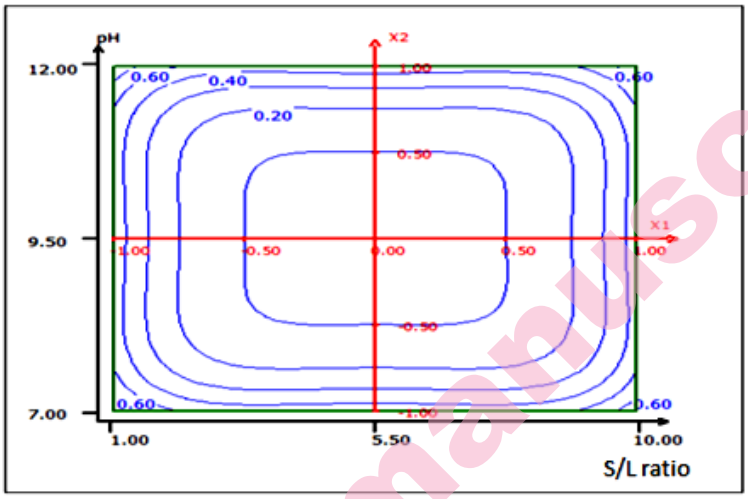

Fig 7. Isovariance by rotation in the S/L ratio, pH plane with: Temperature = 35°C and C = 2.10 g·L^{-1}

To validate the model's accuracy, we carried out experiments on test points located as far as possible from the experimental points. The results of statistical tests performed at these points indicated clearly that the differences between the experimental and predicted responses R_{exp} - R_{the} for each test point fell within the range of experimental error, meaning that they were not statistically significant according to the t-test. Additionally, the coefficient of determination value of 0.94 and the adjusted coefficient of determination value of 0.90 indicated that the model is significant.

To enhance the previous model, the response values obtained from checkpoints were included in the coefficient calculation. The refined model was expressed as follows:

$$R = 58.07 + 0.52\,X_3 - 16.79\,X_5 + 7.57\,X_3^2 \quad (4)$$

Table VIII compares the coefficients of the two models. Most effects remain unchanged after including the test points; however, slight differences have been observed for the intercept effect a_0 and the quadratic effects $a_{2\text{-}2}$, $a_{3\text{-}3}$, and $a_{5\text{-}5}$. A change in sign has been noted for the effect $a_{4\text{-}4}$; this discrepancy is likely due to minor experimental variations. However, the coefficient's value is very small (-0.07), which does not significantly impact predictions or optimization. All these non-significant variations justified the better refining of the model using test points.

TABLE VIII. Model coefficients with and without test points

Coefficient	Without test points	Whit test points
a_0	59.21	58.07
a_2	0.48	0.48
a_3	0.51	0.52
a_4	-1.59	-1.77
a_5	-16.89	-16.79
$a_{2\text{-}2}$	-2.32	-1.88
$a_{3\text{-}3}$	7.10	7.57
$a_{4\text{-}4}$	0.28	-0.07
$a_{5\text{-}5}$	-3.47	-2.83
$a_{2\text{-}3}$	0.49	0.49
$a_{2\text{-}4}$	-0.13	-0.14
$a_{2\text{-}5}$	0.16	0.16
$a_{3\text{-}4}$	0.76	0.76
$a_{3\text{-}5}$	0.11	0.11
$a_{4\text{-}5}$	-1.01	-0.98

Fig. 8 illustrates that the residuals are randomly distributed around zero, showing no discernible pattern. This confirms the validity of the model and indicates a strong agreement between the predicted and the experimental response values.

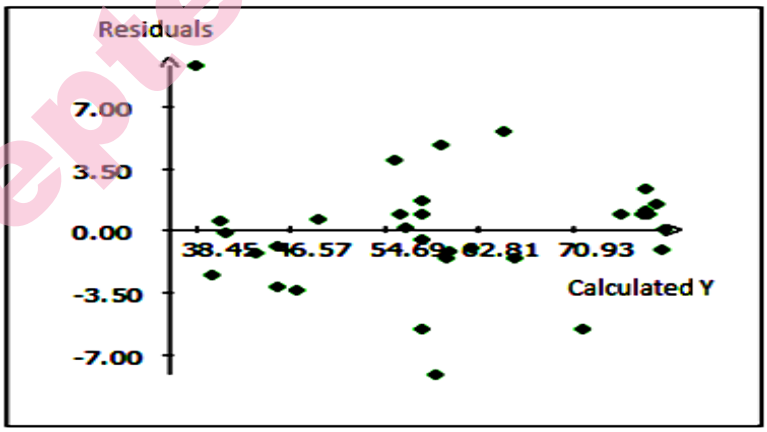

Fig 8. Residuals distribution according to the calculated response R

Furthermore, the variance analysis results applied to the refined model (Table IX) indicated that the probability significance of the risk was greater than 5%. However, the main effect of the regression was significant p-value <0.05 therefore, we concluded that the proposed empirical model was suitable for predicting the removal of PC from OMW.

TABLE IX. Variance analysis results

Source of variation	Sum of squares	Degrees of freedom	Mean square	F ratio	Signifi, %
Regression	5468.30	14	390.59	21.617	< 0.01[b]
Residuals	343.30	19	18.07		
Lack-of-fit	309.13	15	20.61	2.412	20.4
Pure error	34.17	4	8.54		
Total	5811.60	33			

[b] Significant at the level of 99.9 %

Response surface methodology (RSM) and the desirability function were combined to identify the optimal values of the process variables for maximum PC removal, based on the model generated from the experimental data. The optimal conditions and maximum response zone was pinpointed using RSM, while the desirability function provided precise values for these parameters[24].

Fig. 9 (a-f) show the 2D contour plots and the three-dimensional (3D) response surfaces plots which play a crucial role in demonstrating the relationship between independent variables and their corresponding responses while maintaining a variable at the zero-level. Fig. 9(a-b) illustrates a significant interaction between pH and initial PC concentration. The percentage reduction increases with pH, indicating a positive quadratic effect on the response, while it decreases significantly with initial concentration C. The optimal region was found at high pH and low C values, peaking at around pH 12 and C of 1.4 $g \cdot L^{-1}$. The other response surfaces in 9 (c-d) and 9 (e-f) illustrate the effects of temperature and the S/L ratio, which result in only slight variations in response within the studied range. Consequently, these parameters were maintained at their central levels: temperature at 35°C and S/L at 5.5 $g \cdot L^{-1}$. The percentage removal achieved was 82.40%.

Desirability function is a widely used method. The values of this function (d_i) range from 0 to 1. A desirability of 0, referred to as 'elementary desirability,' indicates an unacceptable solution for the selected objective, while a desirability of 1 signifies maximum performance, meaning no further improvement is possible.[45] In our study, the aim was to maximize the removal percentage of PC to achieve a target desirability of 100%.

The desirability function applied to the refined model indicated that the maximum theoretical value of PC removal was 80.85% reached at pH 12, C 1.4 $g \cdot L^{-1}$, S/L 5.58 $g \cdot L^{-1}$ and temperature 35.58 °C; these results align with those obtained using the RMS. To validate the model, a test was carried out by setting the operating parameters at their optimal values; the laboratory findings yielded 80.60 ± 0.44 %, which was quite close to the predicted optimal value. The difference between the experimental and the predicted PC removal was in the range of 5%, confirming the validity of the model.

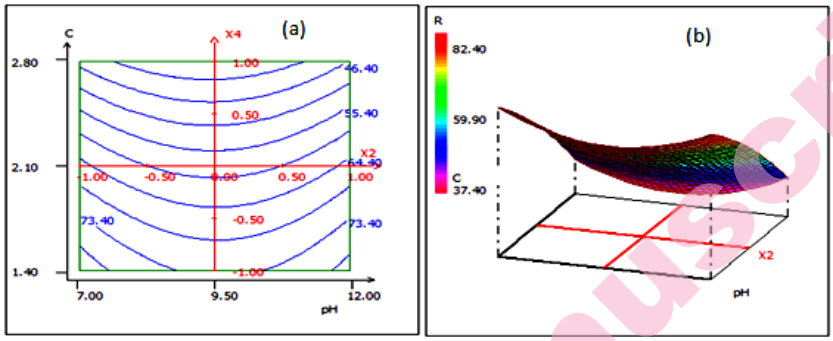

Fig 9 (a-b). The 2D contour plot (a) and the 3D surface plot (b): Interaction effect of pH and C on PC removal, t =35°C and S/L= 5.5 g·L^{-1}

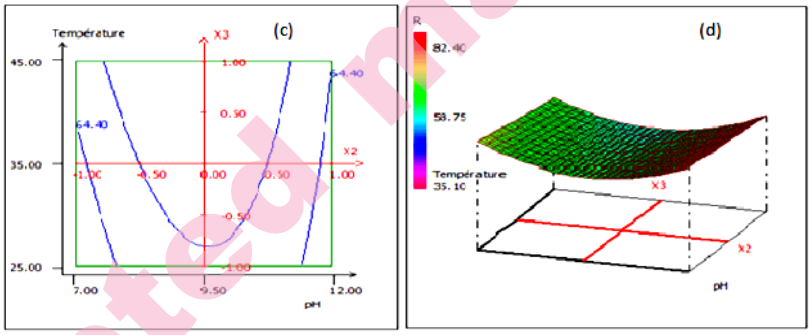

Fig 9 (c-d). The 2D contour plot (c) and the 3D surface plot (d): Interaction effect of pH and temperature on PC removal, C=2.5g·L^{-1} and S/L= 5.5 g·L^{-1}

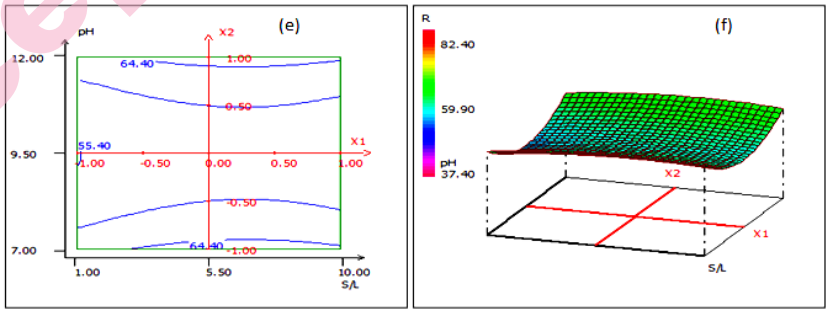

Fig 9 (e-f). The 2D contour plot (e) and the 3D surface plot (f): Interaction effect of pH and S/L ratio on PC removal, t=35°C and C=2.1 g·L^{-1}

Table X summarizes the adsorption efficiency of various adsorbents for the removal of CP from OMW in recent years. The results indicate that the adsorption capacity of Mg-Al LDH (500 °C) powder, studied in this work, is relatively high compared to other adsorbents reported in the literature, such as Zn-Al LDH (500

°C), polymeric resins, zeolite, clay soil, and bentonite. This suggests that Mg-AL LDH is a favorable material for CP removal from aqueous solutions. Additionally, its adsorption capacity is comparable to that of other adsorbents like hydroxyapatite, silicas, and activated carbons, highlighting its potential as an effective alternative for treating liquid effluents.

Table X. Capacities of different adsorbents used for PC removal from OMW

Adsorbent	Conditions	Efficient/%	Reference
Zn-Al LDH (450°C)	Batch experiment, shaking, 25 °C, S/L ratio 1.25 wt/wt, 24 h, natural pH sorbent/sorbate	73	De Martino *et al.*[20]
Activated carbon	Batch experiment, shaking, 25–27 °C, adsorbent dosage 0.45 $g \cdot L^{-1}$	87	Baransi *et al.*[46]
Activated carbon	Batch experiment, 100–450 rpm, 10–50 °C, pH 1.0–10.0, 0–30 min, adsorbent dosage 5–50 $g \cdot L^{-1}$	98	Bouharat *et al.*[47]
clay soil, bentonite and zeolite	Continuous experiment, adsorbent dosage 67 $g \cdot L^{-1}$	67for clay soil,29for bentonite and 37for zeolite	Santi *et al.*[48]
Hydroxyapatite	Batch experiments, 200 rpm, 25 °C, 30 min, pH = 12, adsorbent dosage 10 $g \cdot L^{-1}$	87	Yahiaoui *et al.*[9]
Polymeric resins	Batch experiment, 200–1000 rpm, 25 °C, 1 h, adsorbent dosage 10–200 $g \cdot L^{-1}$	75	Vavouraki *et al.*[49]
Silicas and activated carbon	Batch experiment, 150 rpm, 22 °C, 24 h, adsorbent dosage 60 $g \cdot L^{-1}$	87 for activated carbon, 67–75 for silicas	Yangui *et al.*[50]
Volcanic tuff, natural clay, activated charcoal and combinations	Batch experiment, shaking, 30 °C, 18–24 h, adsorbent dosage 40 $g \cdot L^{-1}$	21–80	Azzam[51]
Mg-Al LDH (500 °C)	Batch experiments, 300 rpm, 5 min pH 12, C 1.4 $g \cdot L^{-1}$, S/L 5.58 $g \cdot L^{-1}$, 35.58°C	80.60 ± 0.44	This work

The LDH recovered from treating OMW under the selected optimal conditions was first dried in an oven at 100 °C for 24 h. It was then calcined in a muffle

furnace at 500 °C for 1 h. Following calcination, the treated LDH was reused for OMW treatment using the adsorption method under optimal conditions.

The reusability of LDH in the adsorption process was evaluated over four consecutive runs and the removal percentages of PC and COD were recorded. As shown in Fig. 10, the percentage of PC removal decreased slightly from 80.60% to 79.4% at the third cycle, remaining stable during the fourth cycle. However, a gradual decline in COD was observed, decreasing from 76% in the first cycle to 67% in the second cycle, and further to 60% and 59% in the third and fourth cycles, respectively. Furthermore, the error bars displayed on the graph indicate that the experimental results are highly reproducible, demonstrating the stability of LDH during its repeated use for PC removal, in contrast of COD which shows significant error variability.

The observed COD removal percentages after each decontamination cycle can be explained by the sorption of phenols and other polar compounds, such as sugars, organic acids, and polyalcohols present in OMW.[20] Additionally, the decline in these reduction rates is likely attributable to the decrease in the LDH pore surface area after each calcination, which is in accordance with reported result.[9]

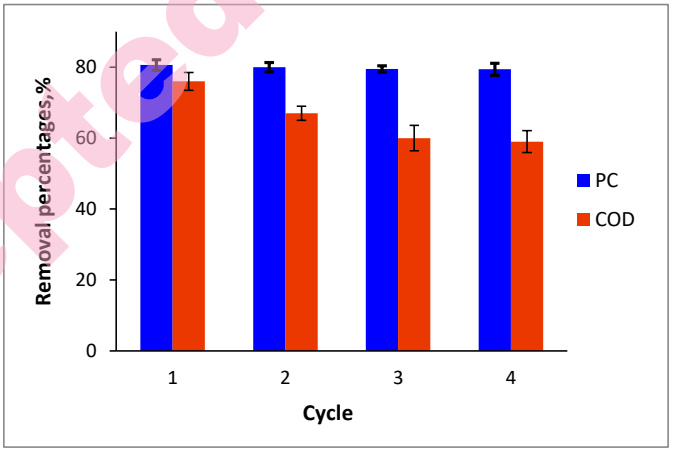

Fig 10. Reusability of the LDH in the adsorption process

CONCLUSION

The optimization strategy by CCD of phenolic compounds removal for OMW treatment with the adsorption process was conducted successfully. The experimental conditions were optimized by considering the effects of some factors, namely S/L ratio, pH, temperature and initial PC content on PC removal using a CCD. The results demonstrated that the predicted values were close to the experimental ones and the high R^2 value confirmed that the accuracy of the proposed polynomial model was acceptable. The regenerability and reusability of

the LDH was confirmed in four successive adsorption batches without producing any new pollution. Therefore, this eco-friendly process is suitable and presents a promising technology for eliminating the organic pollution from wastewaters.

И З В О Д

АДСОРПЦИЈА ФЕНОЛНИХ ЈЕДИЊЕЊА ИЗ ОТПАДНИХ ВОДА НАСТАЛИХ У ПРОИЗВОДЊИ МАСЛИНОВОГ УЉА ПРИМЕНОМ МЕТОДОЛОГИЈЕ ЕКСПЕРИМЕНТАЛНОГ ДИЗАЈНА: СКРИНИНГ И ОПТИМИЗАЦИЈА ЦЕНТРАЛНИМ КОМПОЗИТНИМ ДИЗАЈНОМ

NOUARA YAHIAOUI[1*], RACHIDA DOUANI[1], M'HAND OUGHANEM[1], NOUARA LAMRANI[1†], KAHINA IKKOUR[1,2] И SADIA DEKKAR[1]

*[1]Laboratory of Applied Chemistry and Chemical Engineering, Faculty of Exact Sciences, University Mouloud MAMMERI of Tizi-Ouzou, 15000 Tizi-Ouzou, Algeria * и [2]Laboratory of Physico-Chemical of Materials and Catalysis, Faculty of Exact Sciences, University of Béjaïa, Algeria.*

Методологија експерименталног дизајна примењена је за моделовање и оптимизацију процеса адсорпције у циљу уклањања фенолних једињења из отпадних вода насталих у производњи маслиновог уља, коришћењем двослојних магнезијум-алуминијум-хидроксида (ДХ). Прашкасти ДХ синтетисан је методом копреципитације. Извршена је његова структурна и морфолошка карактеризација. У циљу брзе и ефикасне процене утицаја пет процесних параметара (почетна концентрација фенолних једињења, време контакта, однос чврсте и течне фазе, почетна pH вредност и температура) на ефикасност адсорпције, примењена је Адамарова матрица. Након тога, за оптимизацију процеса адсорпције примењен је централни композитни дизајн, заснован на четири кључна процесна параметра. Коефицијент корелације полиномног модела износио је 94%. Вредности предвиђене функцијом одзива биле су у доброј сагласности са експериментално добијеним резултатима, што потврђује адекватност развијеног модела. Под оптимално дефинисаним експерименталним условима постигнута је максимална ефикасност уклањања фенолних једињења од 80,85%. Могућност поновне употребе регенерисаног ДХ, добијеног калцинацијом на 500 °C, испитана је током четири узастопна циклуса адсорпције при утврђеним оптималним условима. Резултати који се односе на уклањања фенолних једињења као и на хемијску потрошњу кисеоника, показали су да калцинисани ДХ представља перспективну алтернативу за пречишћавање отпадних вода из процеса производње маслиновог уља.

(Примљено 15. новембра 2025; ревидирано 17. јануара 2026; прихваћено 31. јула 2026.)

REFERENCES

1. A. Roig, M. L. Cayuela, M. A. Sánchez-Monedero, *Waste Manag.* **26** (2006) 960 (https://doi.org/10.1016/j.wasman.2005.07.024)
2. M. Niaounakis, C. P. Halvadakis, *Olive Processing Waste Management: Literature Reviewand Patent Survey*,2nded., Elsevier, 2006(https://www.sciencedirect.com/bookseries/waste-management-series/vol/5/suppl/C)

** Corresponding authors: Emails: nouara.yahiaoui@ummto.dz, nouara.lamrani@ummto.dz.

3. A. Moussouni, *Filaha Innove* **4** (2009) 8
4. M. Yalili Kiliç, B. KirilMert, K. Kestioğlu, *UludağUniv. J. Fac. Eng.* **14** (2009) 23 (https://dergipark.org.tr/en/download/article-file/202730)
5. E. Can-Güven, S. Bayrak, B. Dokuyucu, S. Yazici Guvenc, G. Varank, *J. Water Process Eng*. **57** (2023) 104018 (https://doi.org/10.1016/j.jwpe.2023.104018)
6. M. Y. Lee, W. Y. Wang, Y. Duc, H. Y. Hua, N. Huang, Z. B. Xu, Q. Y. Wu, B. Ye, *Chem. Eng. J*. **380** (2020) 122312 (https://doi.org/10.1016/j.cej.2019.122312)
7. Y. Lateb, R. Moussaoui, A. Elias, P. Sharrok, T. Amrouche, *Waste Biomass Valor*. **15** (2024) 7199 (https://doi.org/10.1007/s12649-024-02418-2)
8. A. F. Al Bawab, M. A. Abu Dalo, H. Kanaan, N. Al-Rawashdeh, F. Odeh, *Water Sci. Technol*. **91** (2025) 1529 (https://doi.org/10.2166/wst.2025.007)
9. N. Yahiaoui, H. Kadi, R. Moussaoui, O. Sebaoui, M. Fiallo, *Desalin.Water Treat*. **195** (2020) 232 (https://doi.org/10.5004/dwt.2020.25916)
10. D. Pathania, A. Sharma, Z. M. Siddiqi, *J. Mol. Liq*. **219** (2016) 359 (https://doi.org/10.1016/j.molliq.2016.03.020)
11. V. S. Mane, P. V. Babu, *J. Taiwan Inst. Chem. Eng*. **44** (2013) 81 (https://doi.org/10.1016/j.jtice.2012.09.013)
12. M. Beccari, M. Majone, C. Riccardi, F. Savarese, L. Torrisi, *Water Sci. Technol*. **40** (1999) 347 (https://doi.org/10.1016/S0273-1223(99)00383-2)
13. O. Oukili, M. Chaouch, M. Rafiq, M. Hadji, M. Hamdi, M. Benlemlih, *Ann. Chim.Sci.Mat*. **26** (2001) 45 (https://www.sciencedirect.com/science/article/pii/S0151910701800453)
14. R. Trujillano, *ChemEngineering* **6** (2022) 60 (https://doi.org/10.3390/chemengineering6040060)
15. J. Rocha, M. del Arco, V. Rives, M. A. Ulibarri, *J. Mater. Chem*. **9** (1999) 2499 (https://doi.org/10.1039/A903231B)
16. S. Hamouda, N. Bettahar, M. Aissat, M. Sillanpää, S. AL-Farraj, A. Bahmani, *Catalysts* **15** (2025) 616 (https://doi.org/10.3390/catal15070616)
17. V. Alonso-de-Linaje, M. C. Mangayayam, D. J. Tobler, K. M. Dietmann, R. Espinosa, V. Rives, K. N. Dalby, *Chemosphere* **236** (2019) 124369 (https://doi.org/10.1016/j.chemosphere.2019.124369)
18. D. Wan, H. Liu, R. Liu, J. Qu, S. Li, J. Zhang, *Chem. Eng. J*. **210** (2012) 300 (https://doi.org/10.1016/j.cej.2012.04.088)
19. I. Pavlovic, M. A. González, F. Rodríguez-Rivas, M. A. Ulibarri, C. Barriga, *Appl. Clay Sci*. **80–81** (2013) 76(https://doi.org/10.1016/j.clay.2013.06.008)
20. A. D. Martino, M. Arienzo, M. Iorio, F. Vinale, M. Lorito, D. Paul, P. D. Prenzler, D. Ryan, H. K. Obied, *Appl. Clay Sci*. **53** (2011) 737 (https://doi.org/10.1016/j.clay.2011.07.003)
21. K. Hosni, K. Mahmoudi, M. Haraketi, S. Jellali, E. Srasra, *Comptes Rendus Chimie* **26** (2023) 113 (https://doi.org/10.5802/crchim.265)
22. Z. Zhang, L. Tang, J. Luo, J. Tan, X Jiang, *Adv. Biotechnol.* **4** (2025) (https://doi.org/10.1007/s44307-024-00055-3)
23. W. Mo, C. He, Y. Yang, B. Cheng, J. Yang, Y. Huang, Mater. *Today Sustain.***27** (2024) 100861 (https://doi.org/10.1016/j.mtsust.2024.100861)
24. J. Goupy, Plans d'expériences pour surfaces de réponse, Dunod, Paris, 1999 (ISBN : 978-2-10-003993-7)
25. M. A. Ulibarri, I. Pavlovic, C. Barriga, M. C. Hermosin, J. Cornejo, *Appl. Clay Sci*. **18** (2001) 17(https://doi.org/10.1016/S0169-1317(00)00026-0)

26. J. Macheix, A. Fleuriet, J. Billot, *Phenolic Compounds in Fruit Processing, Chapter 5*in *Fruit Phenolics* (J-J. Macheix, Ed.),CRC Press(1990) (https://doi.org/10.1201/9781351072175)
27. R. L. Plackett, J. P. Burman, *Biometrika* **33** (1946) 305 (https://doi.org/10.1093/biomet/33.4.305)
28. J. Goupy, *Revue de Statistique Appliquée* **38** (1990) 5 (https://www.numdam.org/item/?id=RSA_1990__38_4_5_0)
29. D. Mathieu, J. Nony, R. Phan-Tan-Luu, *NemrodW Software, LPRAI, Marseille*, 2007 (https://www.nemrodw.com/fr/software)
30. F. Z. Mahjoubi, A. Khalidi, M. Abdennouri, N. Barka, *J. Taibah Univ. Sci.* **11** (2017) 76 (https://doi.org/10.1016/j.jtusci.2015.10.007)
31. L. Tabana, S. Tichapondwa , F. Labuschagne, E. Chirwa, *Sustainability* **12** (2020) 4273 (https://doi.org/10.3390/su12104273)
32. R. L. Frost, K. L. Erickson, *Spectrochim. ActaAMol.Biomol. Spectrosc*. **61** (2005) 829 (https://doi.org/10.1016/j.saa.2004.10.012)
33. F. Theiss, A. López, R. L. Frost, R. Scholz, *Spectrochim. ActaA Mol. Biomol. Spectrosc*. **149** (2015) 227 (https://doi.org/10.1016/j.saa.2015.06.002)
34. L. Bünger, K. Garbev, A. Ullrich, P. Stemmermann, D. Stapf, *Membranes* **14** (2024) 170 (https://doi.org/10.3390/membranes14080170)
35. M. Mora, C. Jiménez-Sanchidrián, J. R. Ruiz, *Mater. Lett*. **120** (2014) 82 (https://doi.org/10.1016/j.matlet.2014.01.085)
36. S. Paikaray, M. J. Hendry, *Appl. Surf. Sci*. **258** (2012) 9160 (https://doi.org/10.1016/j.apsusc.2012.09.125)
37. L. P. F. Benício, R. A. Silva, J. A. Lopes, D. Eulálio, R. M. M. Santos, L. Leonardus, L. A. Vergütz, R. F. Novais, L. M. Costa, F. G. Pinto, J. Tronto, *R. Bras. Ci. Solo.* **39** (2015) (https://doi.org/10.1590/01000683rbcs2015081)
38. E. M. Seftel, E. Popovici, M. Mertens, K. De Witte, G. Van Tendeloo, P. Cool, E. F. Vansant, *MicroporousMesoporous Mater*. **113** (2008) 296 (https://doi.org/10.1016/j.micromeso.2007.11.029)
39. L. D. Silva Neto, C. G. Anchieta, J. L. S. Duarte, L. Meili, J. T. Freire, *ACS Omega* 6 (2021) 30119 (https://doi.org/10.1021/acsomega.1c03581)
40. A. Brito, M. E. Borges, M. Garín, A. Hernández, *Energy Fuels* **23** (2009) 2952–2958 (https://doi.org/10.1021/ef801086p)
41. N. K. Lazaridis, *Water Air Soil Pollut*. **146** (2003) 127 (https://doi.org/10.1023/A:1023999303895)
42. M. C. Hermosin, I. Pavlovic, M. A. Ulibarri, J. Cornejo, *Water Res*. **30** (1996) 171(https://doi.org/10.1016/0043-1354(95)00088-3)
43. L. Hu, Z. Li, X. Huang, J. Yhu, I. Hussaini, J. He, X. Chen, *J. Electron. Mater.* **54** (2025) 2167 (https://doi.org/10.1007/s11664-024-11696-4)
44. Z. L. Liu, H. Yu, Y. N. Chen, W. Feng, *Chemistry* **6** (2024) 1523 (https://doi.org/10.3390/chemistry6060092)
45. G. Derringer, R. Suich, *J. Qual. Technol.* **12** (1980) 214 (https://doi.org/10.1080/00224065.1980.11980968)
46. K. Baransi, Y. Dubowski, I. Sabbah, *Water Res.***46** (2012) 789 (https://doi.org/10.1016/j.watres.2011.11.049)
47. D. Bouharat, F. E. Yousfi, A. Ellaghdach, B. D Souhail, N. S Alaoui, *Mediterr J Chem.***7** (2018) 253 (https://doi.org/10.13171/mjc74181101-bouharat)

48. C. A Santi, S. Cortes, L. P. D'Acqui, E. Sparvoli, B. Pushparaj, *Bioresour.Technol.* **99** (2008) 1945 (https://doi.org/10.1016/j.biortech.2007.03.022)
49. A. I. Vavouraki, M. A. Dareioti, M. Kornaros, *Waste Biomass Valor*. **12** (2020) 2271 (https://doi.org/10.1007/s12649-020-01168-1)
50. A. Yangui, M. Abderrabba, *Food Chem.* **262** (2018) 102 (https://doi.org/10.1016/j.foodchem.2018.04.091)
51. M. O. Azzam. *J. Environ. Chem. Eng.* **6** (2018) 2126 (https://doi.org/10.1016/j.jece.2018.03.009).